Structures, energetics, and magnetic properties of Ni_nB clusters with $n=1-8,12$

Mrinalini Deshpande,[1,*] D. G. Kanhere,[1,2] and Ravindra Pandey[1,†]
[1]*Michigan Technological University, Houghton, Michigan 49931, USA*
[2]*Centre for Simulation and Modeling and Department of Physics, University of Pune, Pune 411 007, India*
(Received 20 October 2004; published 9 June 2005)

We report the results of calculations which were performed to investigate equilibrium structures, electronic and magnetic properties of small Ni_nB clusters with $n=1-8,12$ within the framework of density functional theory. The calculated results find that doping of boron enhances the binding energy but reduces the magnetic moments of Ni clusters. The boron prefers to maximize the number of Ni–B bonds by selecting the site which increases the coordination of nickel atoms with B, and is seen to induce significant changes in the geometries of the host clusters for $n<4$. This study also reveals that some of the Ni_nB clusters considered have a substantial higher highest ocupied-lowest unoccupied molecular orbital gap of spin-up electrons as compared to that of spin-down electrons. This may have interesting consequences in the case of the spin-polarized transport, where there will be no conductance for spin-up electrons in such Ni_nB clusters.

DOI: 10.1103/PhysRevA.71.063202 PACS number(s): 36.40.Qv, 36.40.Mr, 61.46.+w, 31.15.Ar

I. INTRODUCTION

During the last few years, much attention has been paid to the study of atomic clusters from both theoretical and experimental sides [1–3]. The areas of interest include ground-state geometries, electronic structure, magnetic, optical, and thermodynamic properties. Small atomic clusters are known to display geometrical arrangements and electronic properties that are significantly different from their bulk properties. In addition, the properties are also found to be strongly dependent on the number of atoms in the given cluster. Many of these properties can be changed by doping the clusters or mixing the clusters with other species. The rich diversity of mixed clusters especially in extended systems has lead to their widespread application in electronics and electrocatalytic processes. In this context, transition metal clusters are of special interest due to their central role in catalysis and magnetism.

It is known that in Ni-based alloys, such as Ni_3Al, the impurities like boron are of particular interest since the boron addition produces remarkable grain-boundary strengthening of $L1_2$ nickel aluminides [4]. Sun *et al.* [5] have studied the effect of boron impurities on the bonding in ordered intermetallic Ni_3Al using the full-potential linear-muffin-tin-orbital method. They found that changes in the electronic structure induced by boron results from the hybridization of the *d*-state of the nearest-neighbor Ni atoms with the B *p*-states. By preferring the Ni-rich octahedral site, boron enhances the intraplanar metallic bonding between Ni atoms which, in turn, effectively enhances the stability of the $L1_2$ ordered intermetallic compound. A similar conclusion was drawn by Painter and Averill [6] on the basis of density functional study of Ni_6B cluster. It may also be noted here that a theoretical study [7] based on a linear combination of atomic orbital approach with density functional formalism find that doping of Fe_n ($n\leqslant 6$) with boron increases the binding energy of Fe_n clusters accompanied with the decrease in their magnetic moments. However, a systematic investigation of the geometries, energetics, and magnetic moment for Ni_nB clusters has not yet been performed. In this paper, we propose to perform such a study of Ni_nB clusters in the size range of $n=1-8$ and 12. These calculations have been carried out by using density functional theory (DFT). In the following section (Sec. II), we describe in brief the computational details, followed by discussion of our results in Sec. III. In Sec. IV, conclusions are given.

II. COMPUTATIONAL DETAILS

All calculations have been performed using first-principles molecular dynamics based on density functional theory. The electronic structure and total energy calculations of all the clusters have been computed using ultrasoft pseudopotentials [8] within generalized gradient approximation given by Perdew-Wang [9] using the VASP package [10]. The clusters were placed in a cubic supercell with an edge of 20 Å, and periodic boundary conditions were imposed. The cutoff energy for the plane wave was set to 241.6 eV. The optimized geometries of the clusters obtained by quenching the various initial configurations using quasi-Newton-Raphson method. The structures were considered to be converged when the force on each ion was less than 0.01 eV/atom with a convergence in the total energy of about 10^{-4} to 10^{-6} eV. In all cases the lowest-energy structure has been confirmed by changing the positions of Ni and B atoms, as well as by considering the configurations of the Ni clusters available from the previous studies [3,11–17]. The stability of the lowest-energy configuration and some of the isomers of a given cluster is further checked by performing calculations in different spin states of a given cluster.

To benchmark the modeling elements of the computational method employed in this study, we have first considered Ni_2 and Ni_{13}, for which theoretical data [3,11–15] are

*Permanent address: Department of Physics, H.P.T. Arts and R.Y.K Science College, Nasik, India.
†Electronic address: pandey@mtu.edu

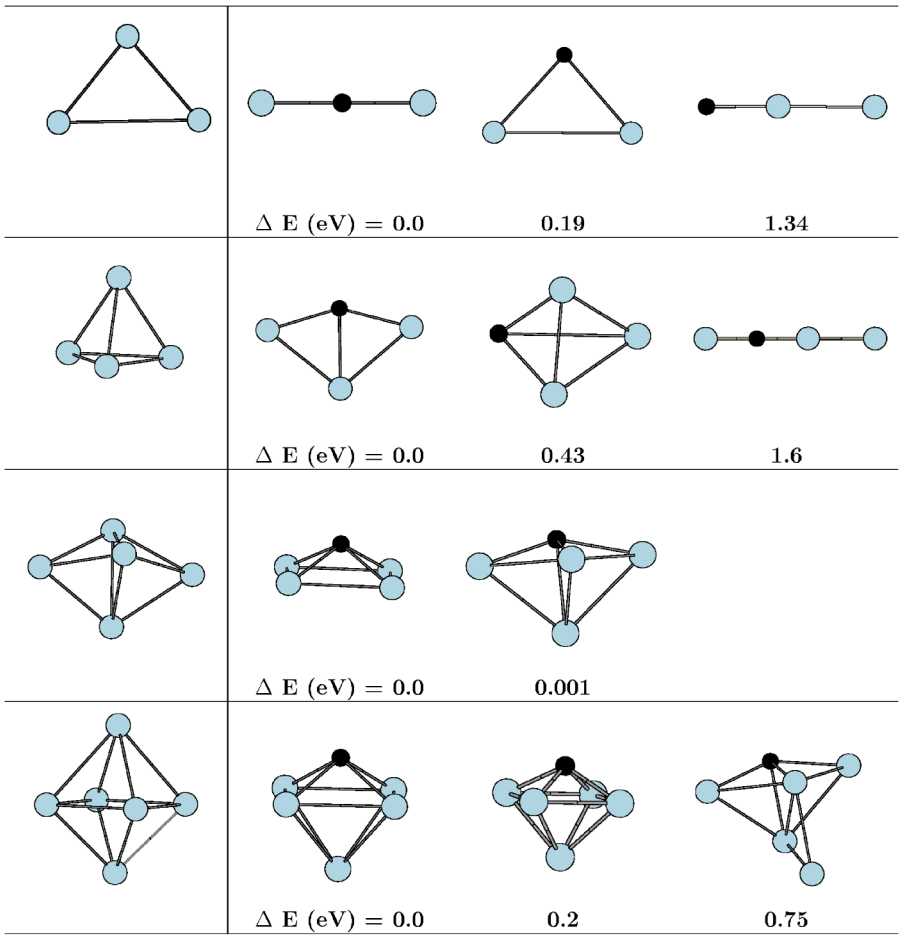

FIG. 1. Ground-state geometries of Ni_{n+1} clusters (column 1). The structures on the right side show the lowest-energy structure (column 2) and some of the low-energy isomers for Ni_nB clusters ($n=2-5$). The lightly shaded spheres represent the Ni atoms and the dark sphere represents the B atom.

available for comparison. Our results are consistent with the earlier theoretical results [11–15] in terms of the computed binding energies (E_b/atom), minimum bondlengths (R), spin multiplicity ($2S+1$), and magnetic moments (μ_B/atom). The calculated total spin-state for Ni_2 is consistent with the matrix isolated cluster measurement [16], while the calculated ground state of Ni_{13} is in agreement with the conclusions inferred from chemical probe experiments [17].

III. RESULTS

In this section, we present the equilibrium structures, stability, energetics, and the magnetic moments of the Ni_nB clusters ($n=1-8,12$). First, we discuss the evolutionary trend of the lowest-energy structures along with some low-lying configurations. The equilibrium structures along with the host Ni_{n+1} geometries are shown in Figs. 1 and 2. Before beginning our discussion, we note that the ionic radius of B atom (1.17 Å) is smaller than that of Ni atom (1.62 Å). Further, the binding energy of Ni–B dimer (2.46 eV/atom) is larger than Ni_2 (1.99 eV/atom) and the dimer bondlengths of Ni–B and Ni_2 are 1.46 and 2.16 Å, respectively.

The lowest-energy structure of Ni_2B turns out to be linear, even though Ni_3 prefers a triangular structure. The isosceles triangle (C_{2v}) is one of the low-lying structures at a slightly higher energy (0.19 eV). The other linear Ni-centered structure (Ni–Ni–B) is well above the lowest-energy configuration (1.34 eV). It has been already noted that for Ni_3 [11], the linear structure is marginally less stable than the triangular configuration. The C_{2v} configuration maximizes the overall number of bonds, but coupling of d-orbitals in triangular symmetry is not optimal for their bonding. To focus on the stability of Ni_2B linear structure, we have examined the isodensity surfaces of the molecular orbitals of both systems. In our discussion to represent the typical occupied molecular orbital we are using the notation HOMO-n, where n represents the number of levels between the highest occupied molecular orbital (HOMO) to that of occupied molecular orbital in the eigenvalue spectrum. Figure 3 shows the isodensity surface for HOMO-8 molecular orbital of the linear configuration where the participation of B p_x is clearly evident. In linear configuration, the B atom hybridizes with the neighboring Ni atoms forming, a Ni–B–Ni bond through hybridization of B p_x with both Ni $d_{x^2-y^2}$. This makes the linear structure more stable compared to the triangular one. The HOMO (not shown) is formed by d-orbitals of nickel.

The lowest-energy structure of Ni_3B is a planar kite-like configuration, while that of Ni_4 is a three-dimensional (3D) tetrahedron. The 3D distorted tetrahedron and the linear configurations of Ni_3B are the other low-lying structures at higher energy, 0.43 and 1.6 eV respectively. Overall, the B atom prefers the planar configuration with the other Ni atoms in Ni_3B, which facilitates hybridization of B p_x and B p_x orbitals with Ni $d_{x^2-y^2}$.

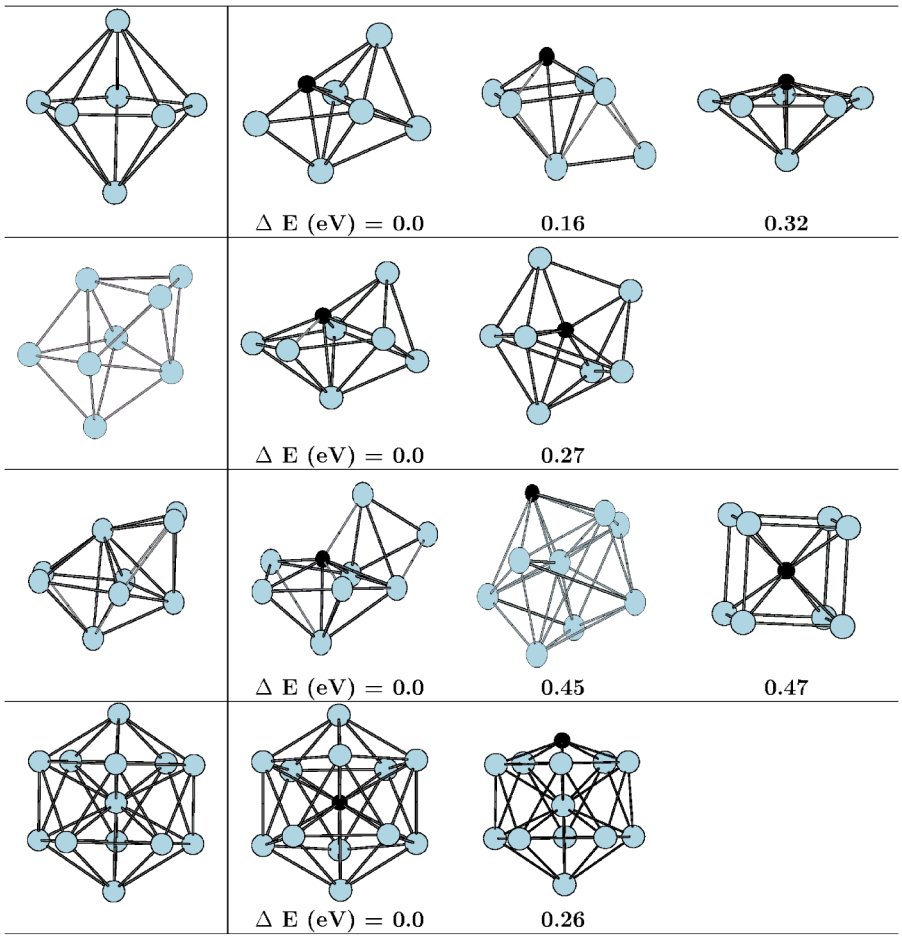

FIG. 2. Ground-state geometries of Ni_{n+1} clusters (column 1). The structures on the right side show the lowest-energy structure (column 2) and some of the low-energy isomers for Ni_nB clusters ($n=6-12$). The lightly shaded spheres represent the Ni atoms and the dark sphere represents the B atom.

Addition of one more Ni atom distorts the planar configuration of Ni_3B to a three-dimensional structure. The lowest-energy structure of Ni_4B is a 3D, square pyramid configuration where the four-coordinated B atom is at its vertex position. The triangular pyramid configuration is nearly degenerate with the square pyramid configuration (0.001 eV). For Ni_5B, the lowest-energy structure is the octahedron configuration with the B atom at the vertex. The next low-lying configuration, 0.2 eV higher in energy, has the same symmetry as that of the lowest-energy structure. Interestingly, we note that the vertex-to-vertex Ni–B distance is 2.53 Å and the Ni–Ni distance is 2.32 Å in the lowest-energy structure. On the other hand, the next low-lying structure shows the respective distances to be 2.50 and 2.34 Å. This clearly indicates that the lowest-energy configuration obtained by our calculations is a result of a delicate balance between the Ni–Ni and Ni–B interactions in Ni_5B.

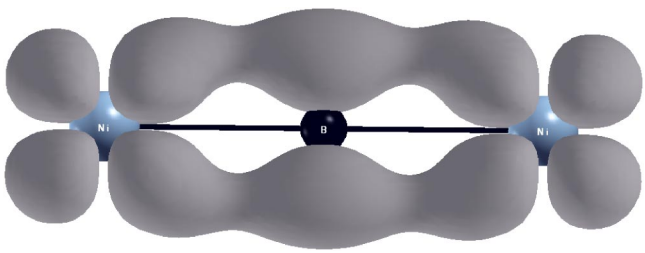

FIG. 3. Isodensity surface corresponding to the HOMO-8 state for lowest-energy configuration of Ni_2B, where the Ni–B–Ni axis is taken as the *Z*-axis.

Ni_6B is a capped octahedron configuration similar to that of the Ni_7 configuration [5]. The capped octahedron but with a different capping position of the Ni atom is nearly degenerate with the lowest-energy configuration (0.16 eV). A pentagonal bipyramid with B at one apex is also found to be one of the low-lying structures (0.32 eV). This trend of capping and distortion continues up to $n=8$. For Ni_nB clusters, the tendency for the formation of a pentagonal ring is also evident for $n>6$. It is interesting to note the B-centered cubic structure of Ni_8B well above the lowest-energy structure (0.47 eV).

For $Ni_{12}B$, we have considered two different sites for the B atom in the icosahedron configuration; one at the center and other at the vertex site of the cluster. The $Ni_{12}B$ structure with B atom at the center is more stable as compared to the vertex position (0.26 eV). The overall evolutionary trend shows that, except for $n=2$ and 3, the geometries of the B-doped cluster are similar to that of Ni_{n+1} where the B atom occupies a substitutional site accompanied with a slight distortion in the cluster.

We now discuss the stability of Ni_nB clusters on the basis of binding energy (E_b). The binding energy (BE) is calculated as

$$E_b[\mathrm{Ni}_n\mathrm{B}] = (-E[\mathrm{Ni}_n\mathrm{B}] + nE[\mathrm{Ni}] + E[\mathrm{B}])/(n+1), \quad (1)$$

where E is the total energy of the system.

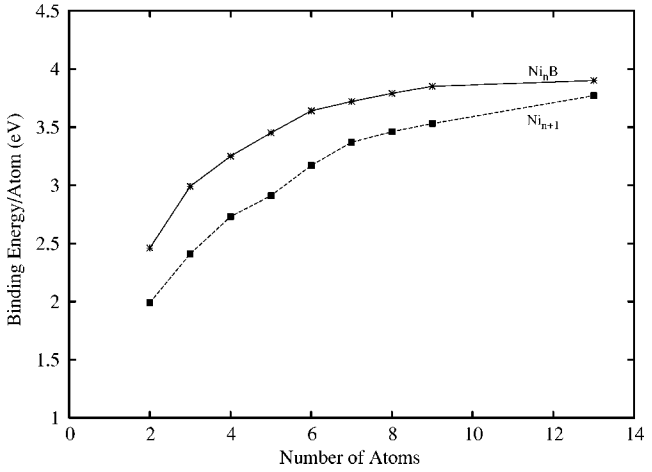

FIG. 4. Binding energy per atom (solid line) for Ni_nB ($n=1-8,12$) and for Ni_{n+1} clusters (dotted line) vs number of atoms in the clusters.

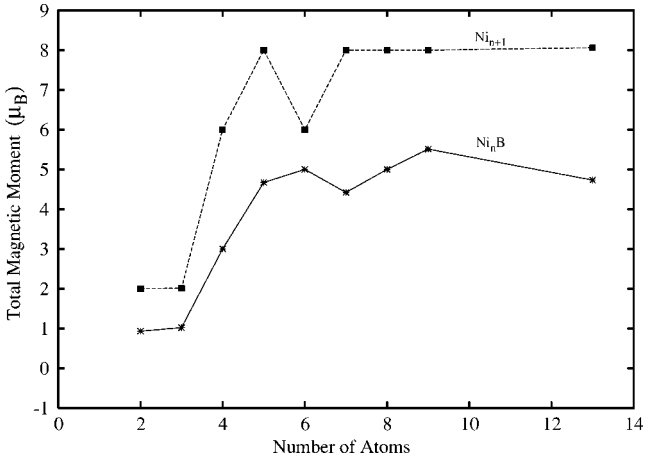

FIG. 5. Total magnetic moment (in μ_B) for the Ni_nB ($n=1-8,12$) and the Ni_{n+1} structures as a function of number of atoms in the cluster.

The binding energy per atom (in eV) for Ni_nB clusters against the number of atoms in the cluster is shown in Fig. 4. For the comparison, we have also plotted the binding energy per atom for host cluster, which clearly indicates that the substitution of the Ni atom by boron enhances the binding energy of the given cluster. For the boron-induced clusters the BE evolves monotonically with total number of atoms in the cluster. For $n<6$, the increase in BE with respect to the host binding energy is by ≈ 1 eV, but for larger clusters the enhancement in the binding energy is small (≈ 0.3 eV). This indicates that the structures are stabilized with the coordination of six Ni atoms for the boron for clusters with $n \geqslant 6$.

Further, the stability of these cluster is also analyzed with respect to their fragmentation into atoms and molecules. The fragmentation channel considered here involves either an Ni atom or Ni_2 molecule. The fragmentation energies are calculated as

$$\Delta E[\mathrm{Ni}_n\mathrm{B}] = E[\mathrm{Ni}_n\mathrm{B}] - (E[\mathrm{Ni}_{n-1}\mathrm{B}] + E[\mathrm{Ni}]), \qquad (2)$$

$$\Delta E[\mathrm{Ni}_n\mathrm{B}] = E[\mathrm{Ni}_n\mathrm{B}] - (E[\mathrm{Ni}_{n-2}\mathrm{B}] + E[\mathrm{Ni}_2]), \qquad (3)$$

where E is the total energy of the system.

Table I shows the fragmentation energies for Ni_nB clusters. For comparison, we have also noted the fragmentation energies of nickel clusters. It clearly indicates the higher stability of Ni_nB clusters against the dissociation compared to that of Ni_{n+1} clusters. It is observed that, for nickel clusters except Ni_4, the energetically lowest fragmentation channel corresponds to the loss of a single Ni atom [11,18]. The boron- induced clusters show a trend similar to that of host clusters. Furthermore, it seems that Ni_6B is relatively unstable with respect to dissociation. In going from Ni_5B to Ni_6B, the bond distance $R_{\mathrm{Ni-B}}$ increases by 5% and decreases by 4% from Ni_6B to Ni_7B. It is seen that boron prefers to maximize the Ni–B interactions by selecting the site that increases the coordination of nickel atoms with B. Even though for Ni_6B the coordination of B atom increases as compared to the Ni_5B cluster, the $R_{\mathrm{Ni-B}}$ distance increases. The decrease in Ni–B interactions makes the cluster relatively unstable.

The total magnetic moment for the Ni_nB clusters against the number of atoms in the cluster is shown in Fig. 5, where we have also plotted total magnetic moment of the host Ni clusters. It can be seen that the doping of the boron decreases the magnetic moment of the host Ni cluster. The reduction in the magnetic moment varies considerably with the size of the cluster, stabilizing to $\approx 5\mu_B$ for $n \geqslant 5$. Some of the higher-energy configurations are found to be with higher magnetic moments than the lowest-energy ones. Thus, the spin state of

TABLE I. Fragmentation energies (eV) of Ni_nB and Ni_{n+1} clusters ($n=1-8$) via loss of a Ni atom and Ni_2 molecule.

		n							
System	Fragmentation path	1	2	3	4	5	6	7	8
Ni_nB	Loss of Ni	4.92	4.06	4.03	4.25	4.54	4.25	4.30	4.28
	Loss of Ni_2	—	5.00	4.11	4.30	4.81	4.82	4.58	4.61
Ni_{n+1}	Loss of Ni	3.98	3.26	3.30	4.07	4.43	4.55	4.16	4.03
	Loss of Ni_2	—	3.26	2.56	4.18	4.52	5.02	4.54	4.21

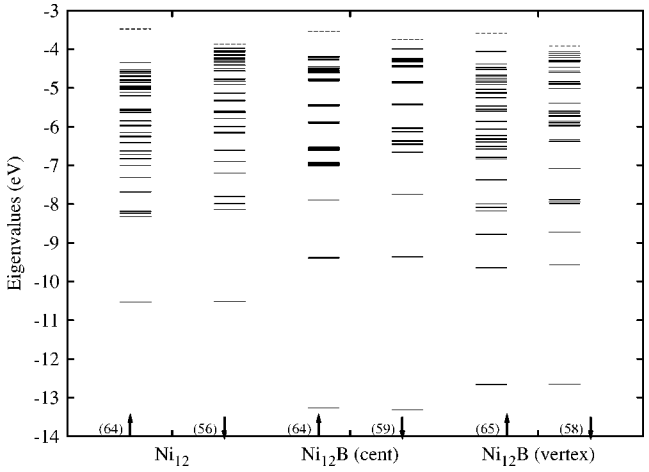

FIG. 6. The eigenvalue spectrum of Ni_{12} and $Ni_{12}B$. The continuous lines represent occupied eigenstates and the dotted one represent the LUMO eigenstate.

the cluster appears to depend on the placement of boron, the configuration of Ni atoms, and the nature of hybridization of Ni d with B p complex. For example, the magnetic moment for the planar configuration of Ni_3B is $3\mu_B$, while for the next low-lying configuration it is $1\mu_B$. In the case of Ni_5B, for the lowest-energy configuration the total magnetic moment is $5\mu_B$ while for the next higher-energy structure it is $3\mu_B$. These remarks are illustrated for $Ni_{12}B$, in which the placement of the B atom changes significantly the magnetic moment of the cluster.

The magnetic moment of boron-centered $Ni_{12}B$ structure is $4.73\mu_B$, while for the vertex-site configuration, it is $8\mu_B$, which is equal to the magnetic moment of the host cluster. A comparison of the eigenvalue spectrum of these three structures (Ni_{12}, $Ni_{12}B$ center, and $Ni_{12}B$ vertex) reveals some interesting features (Fig. 6). The number next to the arrows on the x axis in Fig. 6 refers to spin-up and spin-down electrons. Firstly, upon the induction of boron at the center in Ni_{12}, a noticeable change in the eigenvalue spectrum is seen in terms of well-separated nearly degenerate states. For the vertex B position, however, the nature of the spectrum is similar to that of the host. More interestingly, boron-induced states are well below the HOMO for the lowest-energy configuration of $Ni_{12}B$ center. As a result, the HOMO-LUMO (highest molecular occupied orbital-lowest molecular unoccupied orbital) gap for $\uparrow$-spin in this configuration remains large. As a consequence, three extra electrons associated with B prefer to go in $\downarrow$-state of $Ni_{12}B$. However, in the $Ni_{12}B$-vertex configuration, boron induces an extra state in the spin-up gap as relative to the host Ni_{12} spectrum. This state is then occupied by the extra electrons raising the magnetic moment to $8\mu_B$. It turns out that a B-induced state appears as a HOMO for the apex configuration (see the discussion in the next paragraph).

To discuss the nature of bonding in these clusters, we have examined the charge density isosurfaces of the molecular orbitals and the eigenvalue spectrum (not shown) for the lowest-energy configuration of all clusters. The HOMO of all the lowest-energy configuration belongs to the Ni d and the boron induces the density of states at the middle of the energy spectrum due to the hybridization of B s with Ni d. A typical state from the lowest-energy configuration of $Ni_{12}B$ is shown in Fig. 7. It is seen that the B p hybridized with six Ni d_{z^2}. The next degenerate level, not shown here, B hybridizes with the remaining Ni atoms of the cluster.

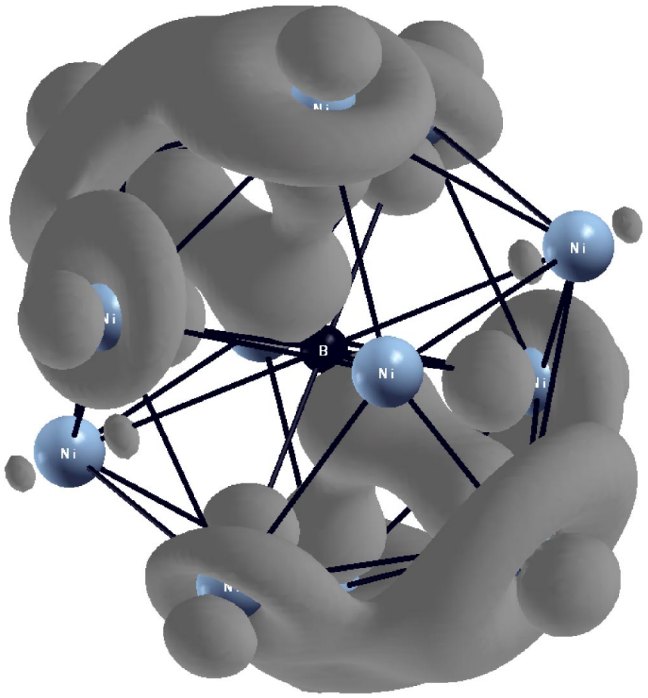

FIG. 7. Isodensity surface corresponding to the HOMO-50 state of $Ni_{12}B$ lowest-energy configuration, where a B atom is at the center site.

Now, we discuss the nature of the HOMO for the two nearly degenerate isomers of $Ni_{12}B$ cluster. As noted earlier, the B-centered icosahedra are lower in energy as compared to B-vertex icosahedra configuration by 0.26 eV. Figures 8(a) and 8(b) show the isodenses for the HOMO's of these two configurations. It can be seen that HOMO is dominated by $d_{x^2-y^2}$ and the boron is not participating in the hybridization for the centered-site configuration. For the vertex configuration, B p_x and B p_y hybridize with five Ni neighbors having d_{z^2} complex; in addition to that B p_z hybridizes with central Ni d_{z^2}, which in turn form a bond with the apex Ni atom. It can be seen that the five neighboring Ni atoms from the lower pentagonal ring participate in the hybridization through $d_{x^2-y^2}$ in HOMO. The consequence of this is leading to the enhancement of the magnetic moment which has already been discussed. Figure 9 shows the spin density $[\rho_\uparrow(\mathbf{r})-\rho_\downarrow(\mathbf{r})]$ for $Ni_{12}B-$vertex configuration. It is seen that, there is no magnetization on boron and central Ni atom. A closer examination of isodenses shows that the distribution of the spin density is inhomogeneous and the maximum moment is observed at vertex Ni atom, which is opposite to the boron.

Now, we bring out an interesting feature of these doped clusters. Figure 10 shows the spin up HOMO-LUMO gap and spin down HOMO-LUMO gap for these clusters. It is seen that, for $n>5$, the boron-doped clusters have a large HOMO-LUMO gap for spin-up electrons ($\approx$1.3 to 2 eV)

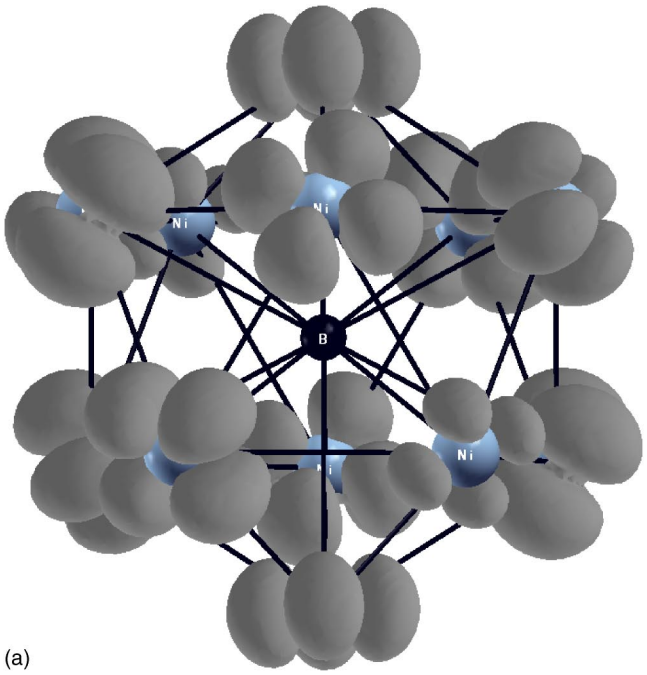

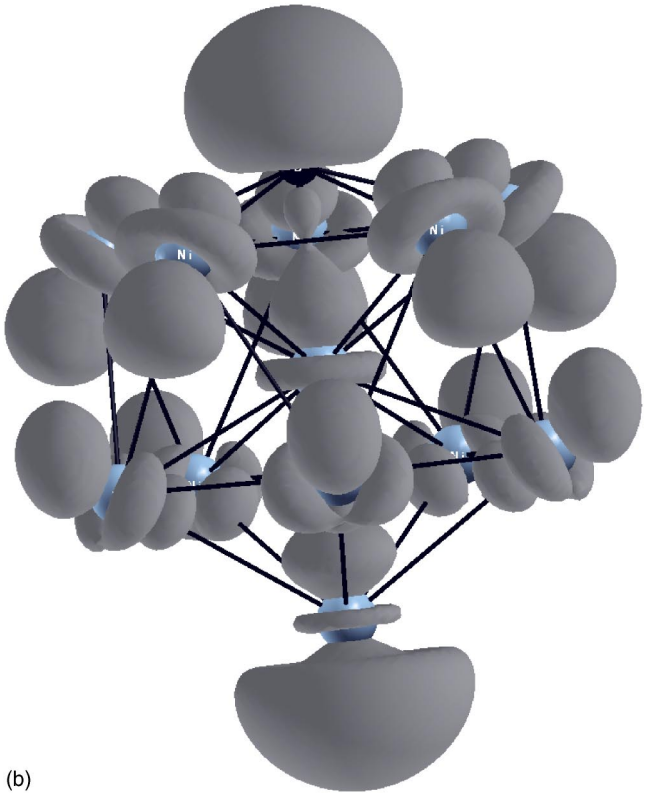

FIG. 8. HOMO isodensity surface (a) for $Ni_{12}B$ center and (b) for $Ni_{12}B$ vertex.

while spin-down electrons have a very small gap ($\approx$0.08–0.43 eV). This will have an interesting repercussion on electron conductance through these clusters. Recently, much attention is being focused on controlled transport of electrons using spin polarization [19–21]. The use of spin degree of freedom adds another dimension to the emerging field of molecular scale electronics (spintronics) [19]. The

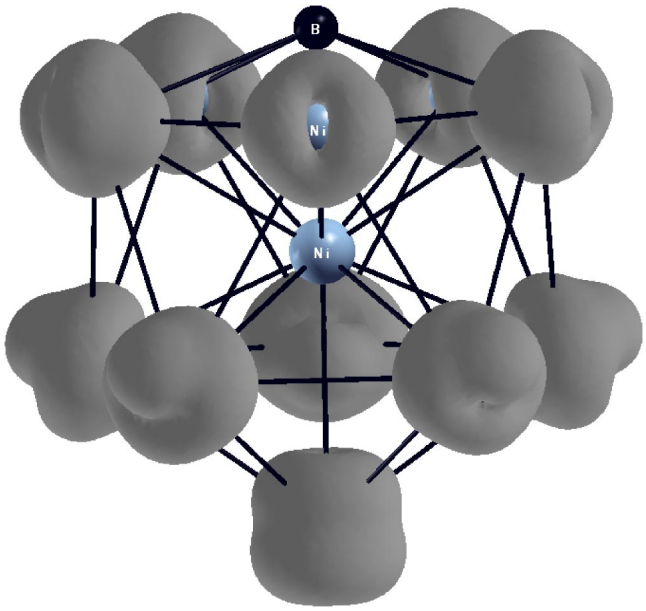

FIG. 9. The spin density $[\rho_{\uparrow}(\mathbf{r})-\rho_{\downarrow}(\mathbf{r})]$ isosurface of $Ni_{12}B$-vertex configuration at one-fifth of its maximum isosurface value.

boron-doped clusters investigated here, having the above-noted property will conduct only through spin down channel (very small spin-$\downarrow$ HOMO-LUMO gap). Therefore, they could be considered as potential candidates in spintronics devices as spin analyzer or spin filter.

IV. CONCLUSIONS

In the present investigation, we have reported the lowest-energy and some of the low-lying configurations of Ni_nB ($n=1-8,12$) using first-principles molecular dynamics. The overall evolutionary trend shows that, except for $n=12$ and 3, the geometries of the doped cluster are similar to that of Ni_{n+1} where the B atom occupies a substitutional site accompanied by a slight distortion in the cluster. The doping of

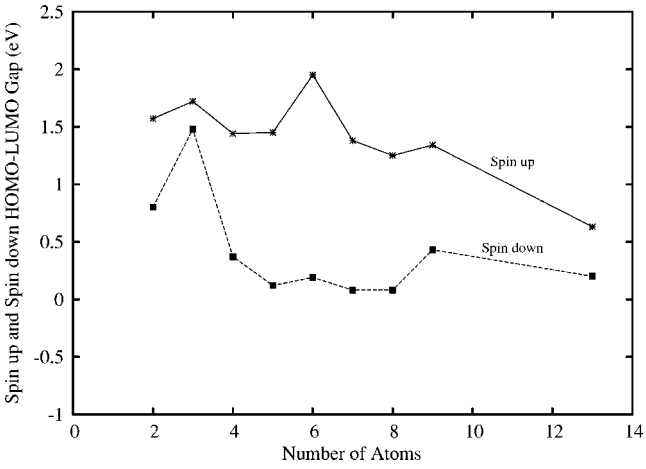

FIG. 10. HOMO-LUMO gap for spin-up (solid line) and spin-down (dotted line) electrons of Ni_nB clusters ($n=1-8,12$).

boron enhances the binding energy but reduces the magnetic moment of the host cluster. This is consistent with the observation that boron in bulk $L1_2$ ordered intermetallic compounds enhances the stability by segregating to the grain boundary than to the free surface. For boron-induced clusters, the structural stability and magnetic properties of these clusters appears to be the outcome of a delicate interplay among the coordination number for B atom, cluster symmetry, and the hybridization of B p and Ni d orbitals. For $n > 5$, the clusters have substantially higher HOMO-LUMO gap for spin-up electrons ($\approx$1.3 to 2 eV) while for spin-down electrons it is very small ($\approx$0.08–0.43 eV). This will have interesting repercussions on electron conductance through these clusters. These clusters will conduct only through a spin-down channel (very small spin-$\downarrow$ HOMO-LUMO gap). Therefore, they could be considered as potential candidates in the emerging field of molecular scale spintronics.

ACKNOWLEDGMENTS

We gratefully acknowledge the Centre for Simulation and Modeling and Department of Physics, University of Pune, India and CSERC, MTU for accessing their computing facility. M. D. D. thanks S. Chacko, M. A. Blanco, and Kah Chun Lau for helpful discussions. M. D. D. and D. K. also gratefully acknowledges Michigan Tech for providing local hospitality.

[1] V. Kumar, K. Esfarjani, and Y. Kawazoe, *Clusters and Nanomaterials*, Springer Series in Cluster Physics (Springer-Verlag, Berlin, 2002).
[2] *Clusters and Nanostructured Materials*, edited by P. Jena and S. N. Behera (Nova Science, New York, 1996).
[3] J. A. Alonso, Chem. Rev. (Washington, D.C.) **100**, 637 (2000).
[4] C. T. Liu, C. L. White, and J. A. Horton, Acta Metall. **33**, 213 (1985).
[5] S. N. Sun, N. Kioussis, S.-P. Lim, A. Gonis, and W. H. Gourdin, Phys. Rev. B **52**, 14421 (1995).
[6] G. S. Painter and F. W. Averill, Phys. Rev. Lett. **58**, 234 (1987).
[7] Q. Sun, X. G. Gong, Q. Q. Zheng, and G. H. Wang, J. Phys.: Condens. Matter **8**, 1805 (1996).
[8] D. Vanderbilt, Phys. Rev. B **41**, 7892 (1990).
[9] J. P. Perdew and Y. Wang, J. Chem. Phys. **45**, 13244 (1992).
[10] Vienna *ab initio* Simulation Package (VASP), Technische Universität Wien, 1999.
[11] F. A. Reuse and S. N. Khanna, Chem. Phys. Lett. **234**, 77 (1995).
[12] F. A. Reuse, S. N. Khanna, and S. Bernel, Phys. Rev. B **52**, R11650 (1995).
[13] S. K. Nayak, S. N. Khanna, B. K. Rao, and P. Jena, J. Phys. Chem. A **101**, 1072 (1997).
[14] B. V. Reddy, S. K. Nayak, S. N. Khanna, B. K. Rao, and P. Jena, J. Phys. Chem. A **102**, 1748 (1998).
[15] S. N. Khanna, M. Beltran, and P. Jena, Phys. Rev. B **64**, 235419 (2001).
[16] M. Moskovits and J. E. Hulse, J. Chem. Phys. **66**, 3988 (1977).
[17] E. K. Parks, L. Zhu, J. Ho, and S. J. Riley, J. Chem. Phys. **100**, 7206 (1994).
[18] L. Lian, C.-X. Su, and P. B. Armentrout, J. Chem. Phys. **96**, 7542 (1992).
[19] R. Pati, L. Senapati, P. M. Ajayan, and S. K. Nayak, Phys. Rev. B **68**, 100407(R) (2003).
[20] M. Ouyang and D. D. Awschalom, Science **301**, 1074 (2003).
[21] K. Tsukagoshi, B. W. Alphenaar, and H. Ago, Nature (London) **401**, 572 (2003).